Supplementary Information:

Hygroscopic Growth of Simulated Lung Fluid Aerosol Particles Under Ambient Environmental Conditions

James F. Davies, Chelsea L. Price, Jack Choczynski and Ravleen Kaur Kohli

1. Analytical Mass Flux Treatment and Settling Times

The analytical treatment of Kulmala et al.,[1] implemented as described by Davies et al.[2] was used to simulate the evaporation of saline particles under 50% RH (fig 1), using the water activity data of E-AIM.[3] While some inaccuracies in the model under these conditions arise due to the temperature correction to account for latent heat of evaporation, this only changes the predicted trends by a few percent. Deposition time was estimated using the terminal velocity of a sphere assuming Stokes law:

$$v = \frac{2}{9}\frac{C\rho g R^2}{\mu}$$

where C is the Cunningham slip correction factor, ρ is the particle density (assumed here to be equal to that of water), g is the gravitational constant, R is the radius, and μ is the dynamic viscosity of air, taken here to be 1.8×10^{-5} Pa s. Stokes law is not applicable for high Reynolds numbers and so for particles sizes above ~100 µm, a slight underestimate of particle suspension time is expected. The Aerosol Calculator (developed by Dr Paul Baron using the equations of Willeke and Baron, Hinds, and accessed via Andrew Maynard)[4–6] was also used to iteratively calculate particle settling times based on Reynolds numbers and drag coefficients.

2. Electrostatic Characterization of Particle Size

In an electrodynamic balance, the gravitational force on the particle is balanced by an upward acting electrostatic force produced by application of a DC voltage to a plate or plate-like electrode. When the particle is stationary, the applied force is equal to the weight and, in the absence of other net forces, the magnitude of the voltage is directly proportional to the mass of the sample, according to:[7]

$$mg = \frac{CqV_0}{2z} \qquad (1)$$

where m is the particle mass, g is the acceleration due to gravity, C is a constant associated with the geometry of the trap (previously determined to be ~0.15)[8], q is the charge on the particle, V_0 is the voltage to balance the particle in the absence of other external forces, and z is the height of the particle above the electrode. In a typical experiment, the mass and charge are not known, but relative changes in the balancing voltage reveal changes in particle mass, under the assumption that the charge is constant, which is verified experimentally.

To control the environmental conditions, an airflow is typically introduced into the EDB chamber. Depending on the internal design of the EDB, this may result in a non-negligible drag force acting on the droplet. For small particles and low flow velocities, the Reynolds number ($Re = \frac{ua}{\nu}$) is <0.1 and Stokes Law describes the magnitude of the drag force. This results in a new force balance equation:

$$mg + 6\pi\chi a\mu u = \frac{CqV}{2z} \qquad (2)$$

where a is the spherical radius of a particle with the same volume as the sample, χ is the dynamic shape factor introduced to scale the drag force experienced by a non-spherical samples to the drag force experienced by a volume-equivalent sphere ($\chi = 1$ for spherical samples), μ is the dynamic viscosity of the gas phase ($\mu = \nu\rho_{gas}$; where ν is the kinematic viscosity and ρ_{gas} is the gas-phase density), u is the gas flow velocity and V is the voltage to balance the particle in the air flow. The relative force contribution from the weight and drag force depends strongly on the size of the particle. Figure S1 shows the weight and drag force as a function of size for a water droplet exposed to various airflow velocities. For small particles (< 5 μm) exposed to gas flows with $u > 10\ cm/s$, the drag force is more than twice that of the weight. Thus, for these particles, the DC voltage is more strongly dependent on the radius rather than the mass. We can relate V-V_0 to radius, while V_0 will be proportional to mass. While optical sizing methods are not typically capable of sizing particles that are sub-micron, the large drag force experienced by small particles may allow their size to be inferred from electrostatic analysis, thus providing a promising method for characterize sub-micron particles in an electrodynamic balance.

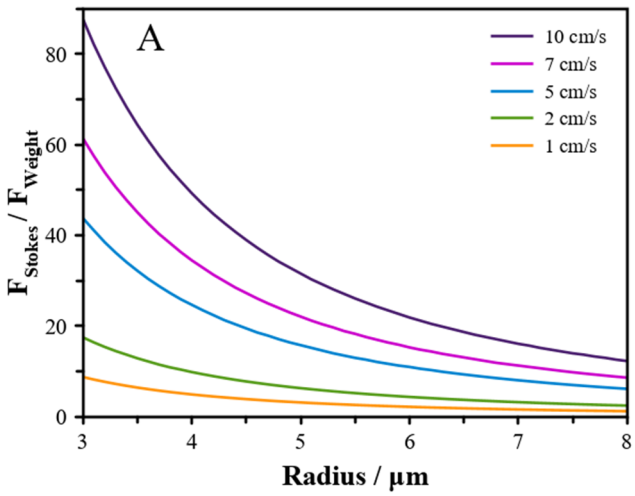

Figure S1: Relative contribution of the Stokes drag force and weight of particle in the LQ-EDB.

For particles of known density and size, we can combine equations 1 and 2, represent the mass using the density and volume ($=\frac{4}{3}\pi a^3$) and solve for the gas flow velocity, according to:

$$u = \frac{2a^2\rho g}{9v}\left(\frac{V}{V_0} - 1\right) \qquad (3)$$

where the charge, height and trap constant have been eliminated.

The radius may only be measured accurately for spherical homogeneous particles. Under dry conditions, these conditions are typically not met, and determining the size of the dry particle can be challenging. If the radius, V, and V_0 are known at a given RH, and V and V_0 are known under dry conditions, then the dry radius of the particle can be estimated:

$$\chi a_{dry} = a_{RH}\frac{V_{dry} - V_{0,dry}}{V_{RH} - V_{0,RH}} \qquad (4)$$

If it is assumed that $\chi = 1$ then this expression may be used to infer the dry particle size allowing radial growth factors to be determined. Mass growth factors may be derived directly from $\frac{V_{0,RH}}{V_{0,dry}}$.

3. Gas Flow Velocity Calibration

We follow the method used by Zhang and Davis[9] to calibrate the airflow velocity using droplets of known density under dry conditions (hexaethylene glycol; $\rho = 1.127\ g/cm^3$). The particle size was determined using Mie theory and Equation 3 was used to determine the velocity from measured V/V_0. The results of the calibration are shown in Figure S2. This calibration was repeated on 3 droplets of varying size and the standard deviation in the mean was 1.4%, within the uncertainty expected due to the resolution of the voltage set-point (~0.05 V).

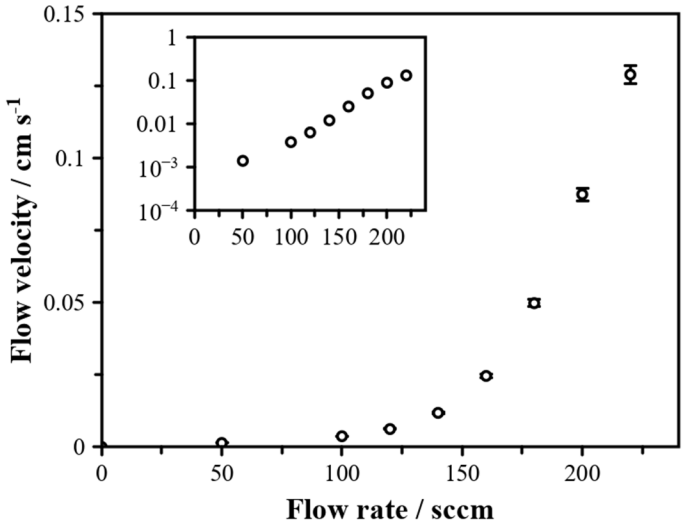

Figure S2: Calibration results of flow velocity in the LQ-EDB following the method described in the text.

4. Glycerol Evaporation

Glycerol droplets are semi-volatile and will shrink over a few hours by steady-state diffusion controlled evaporation.[10,11] Using Mie resonance spectroscopy and the sizing algorithms of Preston and Reid,[12] we determine the radius as a function of time to within 5 nm precision for droplets on the order of 5000 nm. We simultaneously measured the DC voltage required to balance the particle in a gas flow of 20 sccm, as shown in Figure S3A. We compare the time-dependence of the voltage to the expected trend assuming voltage is proportional to mass and see excellent agreement across a mass decrease of a factor of 3. This is consistent with the trend of radius-cubed (i.e. proportional to mass) as shown in the inset of Figure S3A.

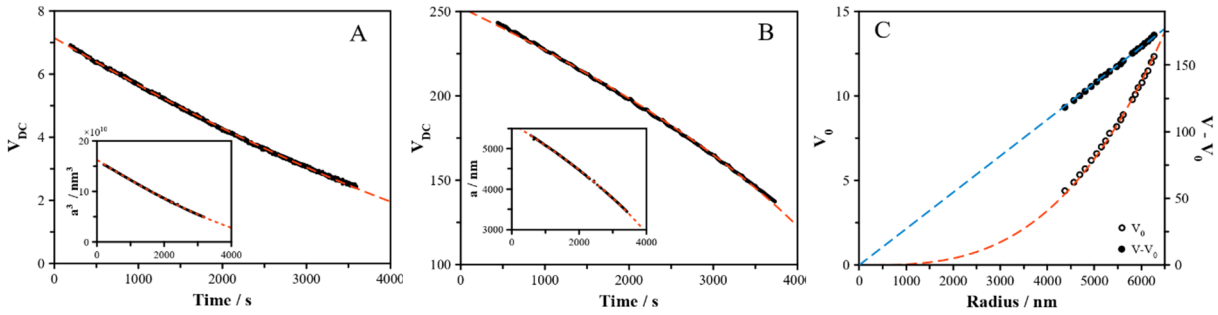

Figure S3: (A) Evaporation of glycerol under zero-flow conditions - V_{DC} is proportional to the mass of the particle. (B) Evaporation of glycerol under 200 sccm flow - V_{DC} is approximately proportional to the radius. (C) V_0 and $V - V_0$ are directly proportion to the mass and size, respectively. Dashed lines indicate linear trend (blue – radius) and cubic trend (red – mass).

We next increased the gas flow to 200 sccm, with a notable increase in the voltage required to balance the droplet, indicating a much larger Stokes drag force. The trend in DC voltage with time for a similar glycerol droplet is shown in Figure S3B. In this case, we see that the square of the voltage varies linearly with time, indicating the voltage is now directly proportional to the radius. Clearly, on going from 20 sccm to 200 sccm we are increasing the Stokes drag to the point where it is the dominant force on the particle. At 200 sccm, the velocity was around 9.3 ± 0.2 cm/s while at 20 sccm the velocity was <0.1 cm/s. The force ratio (F_{drag}/F_{weight}) under high flow conditions is >20, while under low flow conditions, the ratio is <0.25.

In Figure S3C, we look more closely at the dependence of the voltage on size for flow and no-flow conditions. Under flow conditions, we subtract the voltage from the no-flow case and report $V\text{-}V_0$ versus radius, showing a linear relationship that intercept the origin. For V_0 versus radius, we see a cubic dependence that also intercepts the origin, although this is less clear due to a gentle approach to zero.

These data clearly show that the DC voltage varies exactly as expected at the limits of high flow rate and zero flow rate. The density of the particle throughout evaporation is constant and thus these data are straightforward to interpret. For NaCl varying as a function of humidity, both the size and density change, as discussed in the following section.

5. NaCl Hygroscopic Growth

$NaCl_{(aq)}$ droplets have a well characterized hygroscopic response with respect to relative humidity that may be used to further validate our interpretation of the DC voltage. As the RH is decreased, the droplet will lose water and shrink. The efflorescence and deliquescence transitions are also well characterized. In Figure S4A we report the parameter $V\text{-}V_0$ versus the radius derived from Mie resonance spectroscopy and, as in the case of glycerol, we see a linear relationship that intercepts the origin. This further support the radial dependence of the Stokes drag force. In Figure S4B, we deduce the mass growth factor as a function of RH from V_0 measured at elevated RH divided by V_0 under dry conditions. This is compared against the predicted mass growth factor from E-AIM, a well-established aerosol thermodynamic model, with agreement within the uncertainty across the full RH range. We also show the estimated radial growth factor from the DC voltage with a 100 sccm gas flow rate. By using $(V - V_0)$ under dry conditions, the radial growth factor is underpredicted. This is due to the shape of the dry particle (NaCl adopts a cubic morphology and will have a larger Stokes radius than a spherically equivalent volume) and using a dynamic shape factor of 1.075, we achieve agreement within uncertainty.

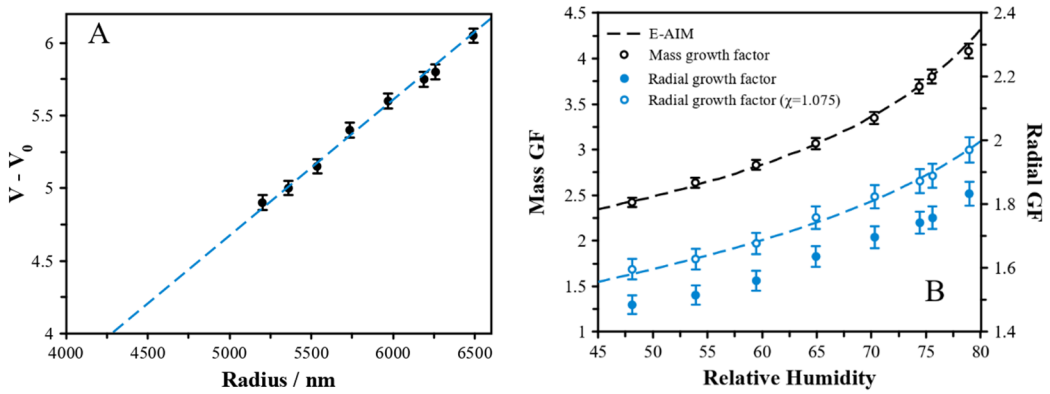

Figure S4: (A) $V - V_0$ is directly proportional to the radius of the particle. (B) Mass GF determined from V_0 and radial GF determined from $V - V_0$, with a shape factor of $\chi = 1.075$ required to account for the non-spherical dry particle.

6. SLF Composition

The SLF mixture was made according to the recipe of Boisa et al.[13] and the composition is detailed in Table S1. The mass balance used to prepare these samples has 0.001 g precision, which reflects in a maximum systematic error of 5% for the components at the lowest contributions. The calculated mass fractions are accurate to around 1 part in 10^{-4}.

Table S1: Simulated lung fluid composition.

Inorganics		
Reagent	**Conc. / g L^{-1}**	**Mass fraction**
NaCl	6.02	0.541
$CaCl_2$	0.256	0.023
Na_2HPO_4	0.15	0.013
$NaHCO_3$	2.7	0.243
KCl	0.298	0.027
$MgCl_2$	0.2	0.018
Na_2SO_4	0.072	0.006

Organics		
Reagent	**Conc. / g L^{-1}**	**Mass fraction**
Ascorbic	0.018	0.002
Uric acid	0.016	0.001
Glutathione	0.03	0.003
Albumin	0.26	0.023
Cysteine	0.122	0.011
DPPC	0.1	0.009
Glycine	0.376	0.034
Mucin	0.5	0.045
Total	11.118	1

7. Estimated Mass Growth Factor of SLF

Under a simple set of assumptions, we can predict the hygroscopic growth of the SLF mixture based on the contributions from NaCl and $NaHCO_3$. Using E-AIM,[3] we obtain the mass fraction of solute for a binary NaCl and water mixture as a function of RH. Given that the mass ratio of each component in the SLF is known, we can estimate the amount of water associated with each hygroscopic component, and assume that the other components contribute negligibly to the water content due to their low mass fraction or low hygroscopicity. If we assume that $NaHCO_3$ is associated with 70% the amount of water as the same mass of NaCl, based on a simple Raoult's law argument, we can sum the total solute and water masses in the mixture to determine the mass fraction of solute:

$$MFS = \frac{m_{NaCl} + m_{NaHCO_3} + m_{non-hyg}}{m_{H_2O,NaCl} + m_{H_2O,NaHCO_3} + m_{NaCl} + m_{NaHCO_3} + m_{non-hyg}}$$

The results of this analysis, along with the E-AIM data for NaCl, are shown in Table S1.

Table S2: Analysis of the hygroscopicity based on assumptions of individual component hygroscopicity. These data are reported in Fig 5.

E-AIM - NaCl									
RH	**Mass GF**	**MFS**	**m_{NaCl}**	**$m_{H2O,NaCl}$**	**m_{NaHCO3}**	**$m_{H2O,NaHCO3}$**	**$m_{non-hyg}$**	**MFS**	**Mass GF**
45.6	2.360	0.424	0.424	0.576	0.193	0.183	0.154	0.504	1.986
46.4	2.380	0.420	0.420	0.580	0.191	0.184	0.153	0.500	2.001
47.2	2.410	0.415	0.415	0.585	0.189	0.186	0.151	0.494	2.022
48.0	2.430	0.412	0.412	0.588	0.187	0.187	0.150	0.491	2.037
48.8	2.450	0.408	0.408	0.592	0.186	0.188	0.148	0.488	2.051
49.6	2.470	0.405	0.405	0.595	0.184	0.189	0.147	0.484	2.066
50.4	2.500	0.400	0.400	0.600	0.182	0.191	0.145	0.479	2.088
51.2	2.520	0.397	0.397	0.603	0.180	0.192	0.144	0.476	2.102
52.0	2.550	0.392	0.392	0.608	0.178	0.193	0.143	0.471	2.124
52.8	2.570	0.389	0.389	0.611	0.177	0.194	0.141	0.468	2.138
53.6	2.600	0.385	0.385	0.615	0.175	0.196	0.140	0.463	2.160
54.4	2.630	0.380	0.380	0.620	0.173	0.197	0.138	0.458	2.182
55.3	2.660	0.376	0.376	0.624	0.171	0.199	0.137	0.454	2.204
56.1	2.680	0.373	0.373	0.627	0.170	0.199	0.136	0.451	2.218
56.9	2.710	0.369	0.369	0.631	0.168	0.201	0.134	0.446	2.240
57.7	2.740	0.365	0.365	0.635	0.166	0.202	0.133	0.442	2.262
58.5	2.780	0.360	0.360	0.640	0.164	0.204	0.131	0.437	2.291
59.3	2.810	0.356	0.356	0.644	0.162	0.205	0.129	0.432	2.312
60.1	2.840	0.352	0.352	0.648	0.160	0.206	0.128	0.428	2.334
60.9	2.870	0.348	0.348	0.652	0.158	0.207	0.127	0.424	2.356
61.7	2.910	0.344	0.344	0.656	0.156	0.209	0.125	0.419	2.385
62.5	2.950	0.339	0.339	0.661	0.154	0.210	0.123	0.414	2.414
63.3	2.980	0.336	0.336	0.664	0.153	0.211	0.122	0.411	2.436
64.1	3.020	0.331	0.331	0.669	0.151	0.213	0.120	0.406	2.465
64.9	3.060	0.327	0.327	0.673	0.149	0.214	0.119	0.401	2.494
65.8	3.110	0.322	0.322	0.678	0.146	0.216	0.117	0.395	2.530
66.6	3.150	0.317	0.317	0.683	0.144	0.217	0.115	0.391	2.559
67.4	3.200	0.313	0.313	0.688	0.142	0.219	0.114	0.385	2.595
68.2	3.240	0.309	0.309	0.691	0.140	0.220	0.112	0.381	2.624
69.0	3.290	0.304	0.304	0.696	0.138	0.221	0.111	0.376	2.660
69.8	3.350	0.299	0.299	0.701	0.136	0.223	0.109	0.370	2.704

70.6	3.400	0.294	0.294	0.706	0.134	0.225	0.107	0.365	2.740
71.4	3.460	0.289	0.289	0.711	0.131	0.226	0.105	0.359	2.784
72.2	3.520	0.284	0.284	0.716	0.129	0.228	0.103	0.354	2.827
73.0	3.580	0.279	0.279	0.721	0.127	0.229	0.102	0.348	2.871
73.8	3.650	0.274	0.274	0.726	0.125	0.231	0.100	0.342	2.921
74.6	3.720	0.269	0.269	0.731	0.122	0.233	0.098	0.336	2.972
75.5	3.800	0.263	0.263	0.737	0.120	0.234	0.096	0.330	3.030
76.3	3.880	0.258	0.258	0.742	0.117	0.236	0.094	0.324	3.088
77.1	3.960	0.253	0.253	0.747	0.115	0.238	0.092	0.318	3.146
77.9	4.050	0.247	0.247	0.753	0.112	0.240	0.090	0.311	3.211
78.7	4.150	0.241	0.241	0.759	0.110	0.242	0.088	0.305	3.284
79.5	4.250	0.235	0.235	0.765	0.107	0.243	0.086	0.298	3.356
80.3	4.370	0.229	0.229	0.771	0.104	0.245	0.083	0.290	3.443
81.1	4.490	0.223	0.223	0.777	0.101	0.247	0.081	0.283	3.530
81.9	4.620	0.216	0.216	0.784	0.098	0.249	0.079	0.276	3.625
82.7	4.760	0.210	0.210	0.790	0.095	0.251	0.076	0.268	3.726
83.5	4.920	0.203	0.203	0.797	0.092	0.254	0.074	0.260	3.842
84.3	5.090	0.196	0.196	0.804	0.089	0.256	0.071	0.252	3.965
85.2	5.280	0.189	0.189	0.811	0.086	0.258	0.069	0.244	4.103
86.0	5.490	0.182	0.182	0.818	0.083	0.260	0.066	0.235	4.255
86.8	5.730	0.175	0.175	0.825	0.079	0.263	0.063	0.226	4.429
87.6	6.000	0.167	0.167	0.833	0.076	0.265	0.061	0.216	4.625
88.4	6.300	0.159	0.159	0.841	0.072	0.268	0.058	0.207	4.843
89.2	6.650	0.150	0.150	0.850	0.068	0.270	0.055	0.196	5.096
90.0	7.060	0.142	0.142	0.858	0.064	0.273	0.052	0.185	5.394
99.5	115	0.009	0.009	0.991	0.004	0.315	0.003	0.012	83.650

1 M. Kulmala, T. Vesala and P. E. Wagner, *Proc. R. Soc. Lond. A*, 1993, **441**, 589–605.
2 J. F. Davies, A. E. Haddrell, R. E. H. Miles, C. R. Bull and J. P. Reid, *The Journal of Physical Chemistry A*, 2012, **116**, 10987–10998.
3 S. L. Clegg, P. Brimblecombe and A. S. Wexler, *J. Phys. Chem. A*, 1998, **102**, 2155–2171.
4 W. C. Hinds, *Aerosol Technology: Properties, Behavior, and Measurement of Airborne Particles*, Wiley-Interscience, New York, 2nd edition., 1999.
5 P. Baron, The Aerosol Calculator, https://therealandrewmaynard.com/2020/05/27/the-aerosol-calculator/.
6 K. Willeke and P. A. Baron, *Aerosol Measurement: Principles, Techniques, and Applications*, Van Nostrand Reinhold, 1993.
7 E. J. Davis and G. Schweiger, *The Airborne Microparticle: Its Physics, Chemistry, Optics, and Transport Phenomena*, Springer Science & Business Media, 2002.
8 J. F. Davies, *Aerosol Science and Technology*, 2019, **53**, 309–320.
9 S. H. Zhang and E. J. Davis, *Chem. Eng. Comm.*, 1987, **50**, 51–67.
10 J. F. Davies, A. E. Haddrell and J. P. Reid, *Aerosol Science and Technology*, 2011, **46**, 666–677.
11 H. K. Cammenga, F. W. Schulze and W. Theuerl, *J. Chem. Eng. Data*, 1977, **22**, 131–134.
12 T. C. Preston and J. P. Reid, *Journal of the Optical Society of America B*, 2013, **30**, 2113–2122.
13 N. Boisa, N. Elom, J. R. Dean, M. E. Deary, G. Bird and J. A. Entwistle, *Environment International*, 2014, **70**, 132–142.